Ultrathin MoO2 Nanosheets Encapsulated in Carbon Matrix for Superior Lithium Storage

Article *in* Nano Energy · November 2014

DOI: 10.1016/j.nanoen.2014.10.027

Nano Energy (2015) 11, 129–135

Available online at www.sciencedirect.com

ScienceDirect

journal homepage: www.elsevier.com/locate/nanoenergy

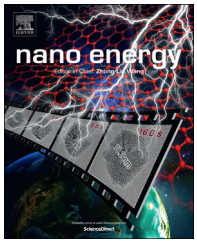

RAPID COMMUNICATION

Ultrathin MoO_2 nanosheets for superior lithium storage

Jiangfeng Ni[a], Yang Zhao[a], Liang Li[a,*], Liqiang Mai[b,*]

[a]College of Physics, Optoelectronics and Energy & Collaborative Innovation Center of Suzhou Nano Science and Technology, Soochow University, Suzhou 215006, China
[b]State Key Laboratory of Advanced Technology for Materials Synthesis and Processing, WUT-Harvard Joint Nano Key Laboratory, Wuhan University of Technology, Wuhan 430070, China

Received 4 September 2014; received in revised form 8 October 2014; accepted 11 October 2014
Available online 7 November 2014

KEYWORDS
Molybdenum dioxide;
Carbon matrix;
Nanosheet;
Lithium storage

Abstract
Ultrathin MoO_2 nanosheets encapsulated in carbon matrix were fabricated through a facile interfacial self-assembly of laminar MoO_3 nanosheets, followed by thermal reduction to MoO_2 mediated by glucose. The resulting MoO_2/C nanosheets exhibited a superior Li-storage capacity, retaining 1051 mAh g^{-1} over 100 cycles at a rate of 0.5 A g^{-1}, and 719 mAh g^{-1} over another 100 cycles at a high rate of 5 A g^{-1} (based on the total mass of MoO_2 and carbon). More importantly, the MoO_2/C nanosheets exhibit robust rate capability, affording a stable capacity of 544 mAh g^{-1} at an extremely high rate of 10 A g^{-1}, thereby suggesting their great potential as promising electrode materials for high power battery applications such as electric automobiles and power tools.

Introduction

In order to meet the requirement for large application such as automobile and clean energy storage, development of battery materials with superior capacity and rate capability is essentially desired. Many nanostructured oxides such as Fe_2O_3, Co_3O_4, and MnO_2 can serve as attractive electrode for Li batteries, owing to their higher theoretical capacity and improved safety versus graphite anode [1]. In particular, rutile structured MoO_2 has received substantial attention due to the high theoretical capacity of 838 mAh g^{-1} (5360 mAh cm^{-3}), superb electronic conductivity ($>1\times10^4$ S cm^{-1}), and facile ion transport property, which all are prerequisites for high-energy and high-power battery applications [2,3].

As bulk MoO_2 generally shows poor Li storage capability due to kinetic barrier[4], diverse nanomaterials such as nanoparticles [5,6], nanowires [7,8], nanorods[9], nanobelts

*Corresponding authors. Tel.: +86 27 87467595; fax: +86 27 87644867.
E-mail addresses: lli@suda.edu.cn (L. Li), mlq518@whut.edu.cn (L. Mai).

http://dx.doi.org/10.1016/j.nanoen.2014.10.027
2211-2855/

[10], and complex assemblies[11–14] have been engineered. These nanoscale materials exhibit upgraded Li-storage performance compared with bulk counterpart, due to higher surface areas, more active sites, and shorter ion diffusion paths [15–17]. However, their rate capability is yet insufficient for practical application and thus needs further improvement. For instance, Huang et al. reported a capacity of 420 mAh g^{-1} at 1.2 A g^{-1} for MoO_2/C nanoparticles [6], while Hu et al. demonstrated a capacity of 260 mAh g^{-1} at 0.84 A g^{-1} for MoO_2 ultrafine nanorods [9]. Possible reasons for the inferior performance may lie in the lacking of efficient electronic/ionic transport pathways and/or inactive confining buffer to accommodate the strain. Recently, graphene supporting represents one of the ideal designs towards high-performance electrodes and has been extensively pursued. Nevertheless MoO_2/graphene nanohybrids still suffered from kinetics barrier, affording a limited rate capability around 400 mAh g^{-1} at a rate of 2 A g^{-1} [18,19]. This might be related to breaking off of conducting pathways by the insulating Li_2O phase and peeling off of active particles from graphene upon Li uptake in MoO_2. On the other hand, the poor kinetics may also be mitigated by fabricating defect-enriched amorphous MoO_2 phase, which could support a high capacity of 705 mAh g^{-1} at the lithiation and de-lithiation rates of 0.1 and 5 A g^{-1}, respectively [20]. However, the poor lithiation capability and the elaborate control of crystalline defects in MoO_2 need to be well addressed before it can be practically utilized [21]. Consequently, it remains challenging for MoO_2 to attain large capacity at high current rates.

In this work, we designed ultrathin MoO_2 nanosheets encapsulated in carbon matrix (designated as MoO_2/C) to drastically raise the capacity and rate capability. With respect to other structures, the nanosheets possess a short ion solid diffusion length, a high electrode/electrolyte interfacial area, and efficient electronic transport pathways [22–25]. As a result, the MoO_2/C nanosheets exhibit superior Li-storage capability, delivering 1051 and 719 mAh g^{-1} over 100 cycles at rates of 0.5 and 5 A g^{-1} respectively. At an extremely high rate of 10 A g^{-1}, the MoO_2/C still affords a capacity of 544 mAh g^{-1}, dramatically outperforming previously reported molybdenum dioxide nanostructures.

Experimental section

Synthesis of MoO_3 nanosheets

Molybdenic acid (Sinopharm, 300 mg) was dispersed in deionized water (15 ml) with continuous stirring. To this suspension t-dodecanethiol (Sinopharm, 3 ml) was introduced and agitated by sonication for 30 min. Afterward, the mixture was transferred to autoclave and reacted at 190 °C for 12 h. The resulting dark precipitation was then collected, washed and dried in vacuum.

Synthesis of MoO_2/C nanosheets

The obtained MoO_3 sheet sample was impregnated with glucose solution (0.1 M) by stirring overnight. The impregnated material was then collected, dried, and finally heated at 400 °C for 1 h under N_2 atmosphere to thermally reduce MoO_3 and to decompose glucose as well.

Material characterization

The molybdenum oxides were characterized by XRD (Rigaku Dmax-2400), SEM, (Hitachi SU-8010) and TEM (FEI Tecnai G2 T20), Raman spectroscopy (Horiba JY LabRAM ARAMIS), TG analysis (Seko TG/DTA-7300), and nitrogen adsorption and desorption isotherms (Micromeritics Tristar 3020).

Electrochemical evaluation

Li-storage performance of MoO_2/C nanosheets was electrochemically evaluated using composite electrodes consisting of 80% active material, 10% Super-P-Li carbon black, and 10% polyvinylidene fluoride binder. The typical loading of active materials is 1.5–2.0 mg cm^{-2}. The counter and reference electrodes are Li metal foil, the electrolyte is 1 M $LiPF_6$ solution in ethylene carbonate and dimethyl carbonate (1:1 by volume), and the separator is glass fiber membrane (Whatman). Cyclic voltammetry (CV) and electrochemical impedance spectroscopy (EIS) were performed on an electrochemical workstation (Zahner Zennium). Galvanostatic tests were conducted on a Land CT2001A battery test system at room temperature.

Results and discussion

The synthesis of MoO_2/C nanosheets involves interfacial self-assembly of laminar MoO_3 nanosheets followed by thermal reduction to MoO_2 mediated by glucose, as schematically elucidated in Figure 1a. In the first step, introduction of t-dodecanethiol to water leads to formation of an immiscible two-phase system. A distinct oil-water interface is then constructed, with the hydrophilic –SH ends arranging towards water while the hydrophobic alkyl groups away from water. During the hydrothermal process, MoO_3 sheets can be assembled at the oil-water interface driven by high temperature and pressure, as Mo has a strong tendency to coordinate with sulphur-ending molecules [26]. More MoO_3 sheets are then stacked up in the [010] direction to form a few-layered sheet structure with van der Waals forces [27,28]. Finally, the MoO_3 nanosheets were then thermally converted to MoO_2/C by glucose through impregnation-reduction-carbonization process [6].

The assembled MoO_3 nanosheets were observed by scanning electron microscopy (SEM) and transmission electron microscopy (TEM), as shown in Figure 1b–d. The MoO_3 sample shows a foam-like structure with abundant pores. Structural wrinkles and corrugation suggest that the foam is composed of ultrathin sheets (Figure 1b, c). Most sheets consist of 3–10 layers with thickness of only 2–7 nm. The structural feature of ultrathin sheet combined with enriched pores built from the stacking of nanosheets is beneficial to rapid Li intercalation and diffusion [9]. The lattice fringe spacing of 0.69 nm coincides with the (020) facets of laminar MoO_3. Additional experiments show the key role that reaction time plays in the formation of nanosheets (Supporting information Figure S1). After impregnation with glucose solution and then heating at 400 °C for 1 h, the porous structure (Figure 1e, f) with nanosheet morphology

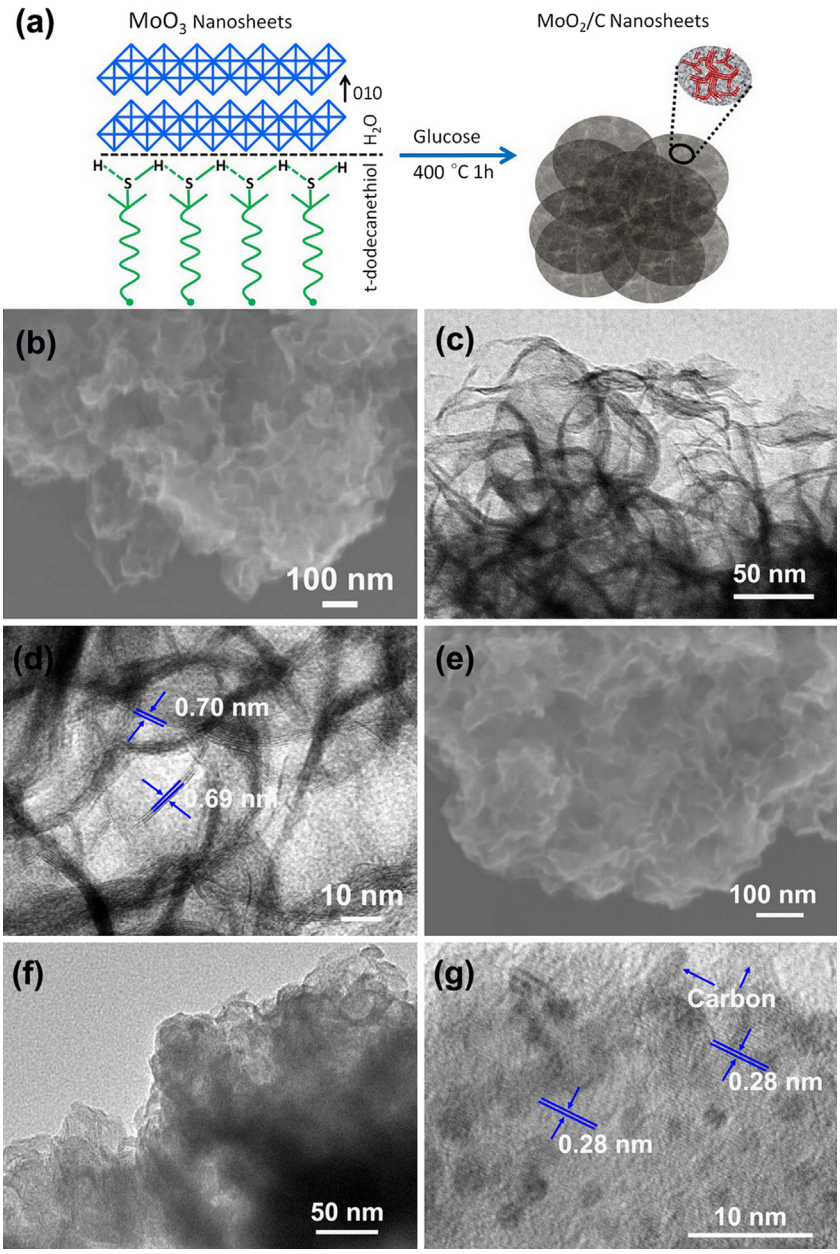

Figure 1 (a) Schematic illustration of synthesis of MoO_2/C ultrathin nanosheets. (b) SEM and (c, d) TEM images of MoO_3 nanosheets. The interplanar spacing of 0.69 nm shown in (d) corresponds to the (020) facet of laminar MoO_3. (e) SEM and (f, g) TEM images of MoO_2/C nanosheets. The spacing of 0.28 nm shown in (g) corresponds to the (−102) plane of monoclinic MoO_2.

(Figure S2) is well preserved. Amorphous phase in the edge of nanosheets could be attributed to carbon (Figure 1g). The interplanar spacing of 0.28 nm (d_{-102}) and energy dispersive X-ray spectroscopy (EDS, Figure S3) confirm that the MoO_3 has been converted to monoclinic MoO_2.

Both MoO_3 and MoO_2/C nanosheets were characterized by X-ray diffraction (XRD) analysis, as presented in Figure 2a. The XRD patterns confirm that the hydrothermal sample can be unambiguously indexed into orthorhombic MoO_3 phase (JCPDS ♯ 05-0508), while the thermally converted sample is monoclinic MoO_2 (JCPDS ♯65-5787). Peaks due to crystalline carbon are barely visible in the MoO_2/C material, suggesting its amorphous state at low heating temperature. Structure of the MoO_2/C probed by Raman spectroscopy is illustrated in Figure 2b. Characteristic bands due to bond vibration modes of molybdenum oxide are clearly confirmed at 990 (Mo=O), 816 (O-Mo-O), 735 (O_2-Mo) and 567 cm^{-1} (O_1-Mo). The finger bands at 355, 283 and 197 cm^{-1} can be assigned to the phonon vibration modes of MoO_2 [29,30]. The additional bands at 1315 and 1564 cm^{-1} can be attributed to D and G bands of carbon. Based on the thermal gravimetric (TG) analysis in air (Figure S4), the loading of carbon in the MoO_2/C is estimated to be 18.2 wt%. In addition, the N_2 adsorption and desorption isotherms of the MoO_2/C reveals a specific surface area of 31.4 $m^2\ g^{-1}$, and pore volume of 0.11 $cm^3\ g^{-1}$ with an average pore size at 3.2 nm, which is particularly beneficial to rapid Li uptake/release (Figure 2c and d).

As suggested above, the porous, ultrathin structure may endow MoO_2/C with superior Li-storage properties. The electrochemical Li-storage performance is probed by CV and galvanostatic tests. In the CV profile (Figure 3a), two highly reversible redox pairs at 1.55/1.71 V (versus Li/Li^+, unless otherwise stated) and 1.26/1.42 V represent the phase transitions from the monoclinic to the orthorhombic phase and then to monoclinic phase, respectively [11]. The phase transition represents Li addition into MoO_2 lattice, with the limit amount being one Li per formula MoO_2. The

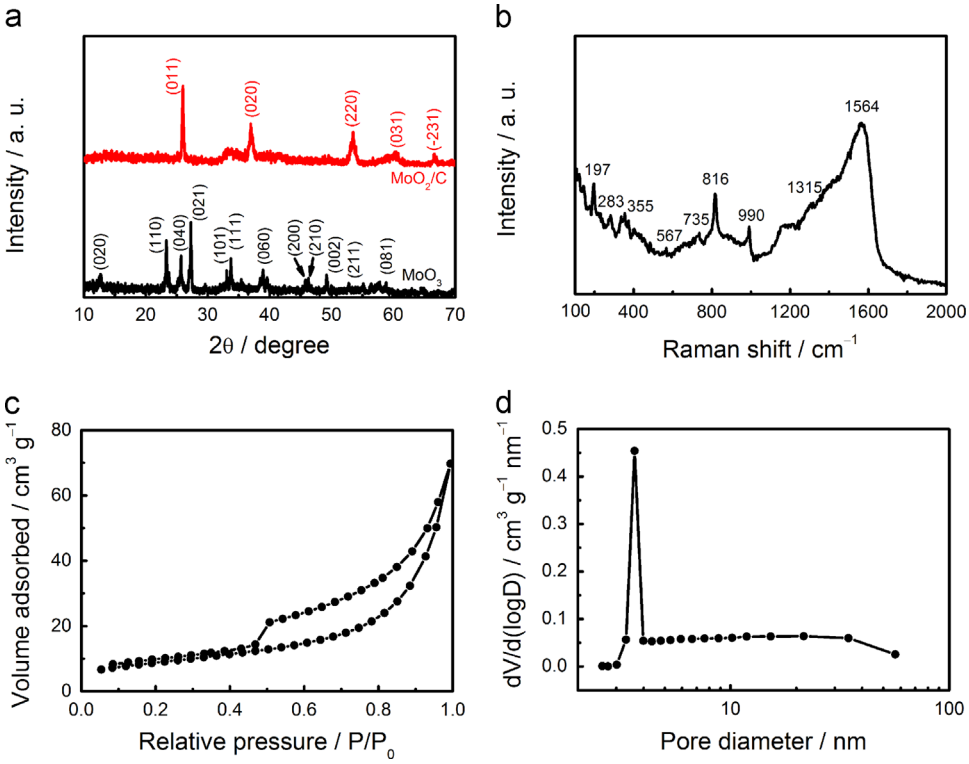

Figure 2 (a) XRD patterns of MoO_3 and MoO_2/C nanosheets. (b) Raman spectroscopy, (c) N_2 adsorption and desorption isotherms, and (d) pore size distribution of MoO_2/C nanosheets.

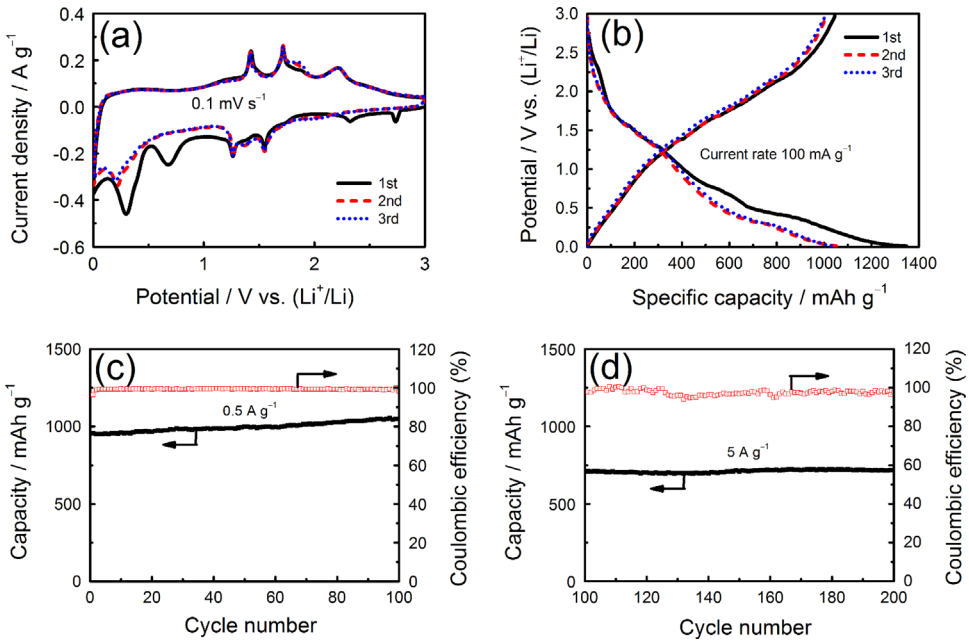

Figure 3 (a) Cyclic voltammograms and (b) charge and discharge profiles of MoO_2/C nanosheet electrodes during initial cycles. (c), (d) Cycling performance of MoO_2/C nanosheets. The MoO_2/C electrodes were firstly cycled (c) at 0.5 A g^{-1} for 100 cycles followed by (d) cycling at 5 A g^{-1} for another 100 cycles. The electrodes were activated at 0.1 A g^{-1} prior to cycling test.

prominent cathodic peak at around 0.29 V reflects conversion reaction, where lithiated MoO_2 was further reduced to metallic Mo through three-electron reduction [5]. Thus, the conversion reaction contributes most capacity. The additional peak at 0.7 V is associated with the formation of solid electrolyte interphase (SEI), while the peak at 2.32 V might be related to MoO_{3-y} phase due to exposure of MoO_2 nanosheets to air [18,31]. These peaks disappear in the subsequent cycles, constituting the major source responsible for the irreversible loss.

The MoO_2/C nanosheets affords a discharge capacity of 1348 mAh g^{-1} and charge capacity of 1045 mAh g^{-1} in the first cycle (Figure 3b). The initial Coulombic efficiency (CE) reaches ~78%. In the following cycles, the reversible capacity stabilizes at 1030 mAh g^{-1}, while the CE drastically rises up to above 95%. Both the reversible capacity level and CE are significantly higher than reported values in literature, as most MoO_2 materials exhibited reversible capacities of 600–800 mAh g^{-1} with initial CE below 70% [6,7,9-13,18,20]. Although the pure MoO_2 prepared by reducing MoO_3 nanosheets with Ar/H_2 delivers a comparable discharge capacity, neither reversible capacity nor CE is comparable to the carbon coated nanosheets (Figure S5). It is worth noting that this practical capacity of MoO_2/C nanosheets surpasses the theoretical value of 838 mAh g^{-1}, which is quite common for carbon modified oxides and may be associated with MoO_{3-y} phase [31], mesopores [6], and carbon matrix [32]. For instance, carbon-encapsulated MnO delivered a much higher capacity of 1268 mAh g^{-1} over the theoretical value of 756 mAh g^{-1} [32].

Moreover, the MoO_2/C nanosheets exhibits impressive stability upon prolonged cycling, regardless applied current rate. As shown in Figure 3c, the nanosheet electrodes retain 1051 mAh g^{-1} with CE nearly 100% at rates of 0.5 A g^{-1} over 100 successive cycles, even surpassing the initial capacity of 957 mAh g^{-1}. Capacity increasing upon cycling is a common phenomenon for oxide and chalcogenide anodes, and generally attributed to activation of materials induced by structural evolution [9,11], crystalline defects [33], and/or surface SEI layer [34]. The electrodes are further tested for another 100 cycles at a high rate of 5 A g^{-1} (Figure 3d), an amazing capacity retention of 719 mAh g^{-1} is demonstrated. To understand such ultrastability, EIS of the MoO_2/C electrodes before and after 100 cycles was measured and compared in Figure S6. The nearly unchanged spectra suggest that charge transfer within nanosheet electrode has barely been affected upon Li cycling. The reduced spike line in the low frequency signals enhanced Li diffusion, which may account for the increased capacity. Additional post TEM observation confirms that the MoO_2 crystallites can be recovered after 100 cycles, eliminating possible pulverization for capacity loss (Figure S7).

In addition to the excellent cycling, the MoO_2/C nanosheets also exhibit outstanding rate capability. As shown in Figure 4a, the hybrid electrodes can afford capacities of 1003, 939 874 and 706 mAh g^{-1} at identical charge-discharge rates of 0.25, 0.5, 1, and 5 A g^{-1}, respectively, with similar charge and discharge profiles (Figure S8). When the current is further increased to 10 A g^{-1}, a capacity of 544 mAh g^{-1} (53% of the reversible 1030 mAh g^{-1} at 0.1 A g^{-1}), or roughly 3480 mAh cm^{-3}, can be achieved. This corresponds to charge and discharge time of 3 min (20C), sufficient for high-rate applications such as electric automobiles and power tools. By contrast, the MoO_3 nanosheets only deliver capacities of 157 and 83 mAh g^{-1} at rates of 5 and 10 A g^{-1}, which may result from the poor conductivity of MoO_3 and lack of carbon buffer (Figure S9). More importantly, when the rates are gradually reduced, a high capacity of 1039 mAh g^{-1} is accordingly restored at 0.25 A g^{-1}. Also, increased capacity is found when the electrodes are further cycled at a constant rate of 0.5 A g^{-1}, implying a superior stability. Clearly, such MoO_2/C nanosheets outperform any reported MoO_2 materials [5-7,9-14,18-20], and other oxides and chalcogenides such as MoO_3/C microballs [35], MoS_2 nanosheets on CNT [36], and FeS/C nanosheets[37] (Supporting information Table S1), verifying effectiveness of our nano-engineering strategy.

Figure 4b shows that the MoO_2/C nanosheets can sustain rapid potential sweep, again proving their robust Li-storage behavior. When the peak currents are logarithmically plotted versus scan rates in Figure 4c, a linear relationship can be clearly observed, with the slopes of 0.89 and 0.83 for the cathodic and anodic processes, respectively. Generally, a slope value of 0.5 suggests a battery behavior where the Li intercalation process is diffusion controlled, whereas a value of 1.0 indicates a capacitive process, which is surface process [38,39]. Here, values of 0.89 and 0.83 indicate that the MoO_2/C nanosheet is more like a pseudocapacitive material rather than a battery one [40]. Similar pseudocapacitive performance has also been reported for MoO_2 nanorods [41], MoO_3 mesoporous thin film [38] and Nb_2O_5 nanocrystal [39]. This assumption can be further convinced by the EIS spectrum, where the phase $>45^\circ$ at low frequency indicates a typical capacitive process. (Figure S10).

Such a robust Li-storage property can be understood based on unique architecture consisting of MoO_2 nanosheets dispersed within carbon matrix. The thickness of nanosheets is only 2–7 nm, which greatly reduces the electron and ion transport path and charge transfer resistance. Meanwhile, the metallic MoO_2 nanosheets provide large accessible surface area for fast ion and electron transport and charge transfer, which lowers the actual areal current flow and polarization. In addition, the two-dimensional, conductive MoO_2 sheets serve as efficient electron transport pathway, which decreases the internal resistance of MoO_2/C electrodes and enables fast charge flow to meet high-rate charge and discharge. Moreover, the unique sheet-in-matrix architecture effectively prevents the aggregation of MoO_2 nanosheets and consequently, retaining a highly accessible area for Li uptake/release upon cycling [7,13]. This is particularly important as many nanomaterials showed improved cycle and rate capability after carbon modification, although the carbon is amorphous and poorly conductive in nature [6]. In a similar way, Zhang et al. utilized amorphous carbon to prevent restacking of graphene nanosheets and achieved a high Li-storage capability [42]. It is also interesting to note that the thin carbon matrix is intrinsically flexible, which can efficiently buffer the volume variation and retain the integrity of nanosheets. This further ensures that most MoO_2 nanosheets are accessible to Li storage upon repeated cycles [43]. These factors work together to lead to an excellent Li-storage property for MoO_2/C nanosheets.

Conclusion

In conclusion, ultrathin MoO_2 nanosheets encapsulated in carbon were readily fabricated via interfacial self-assembly

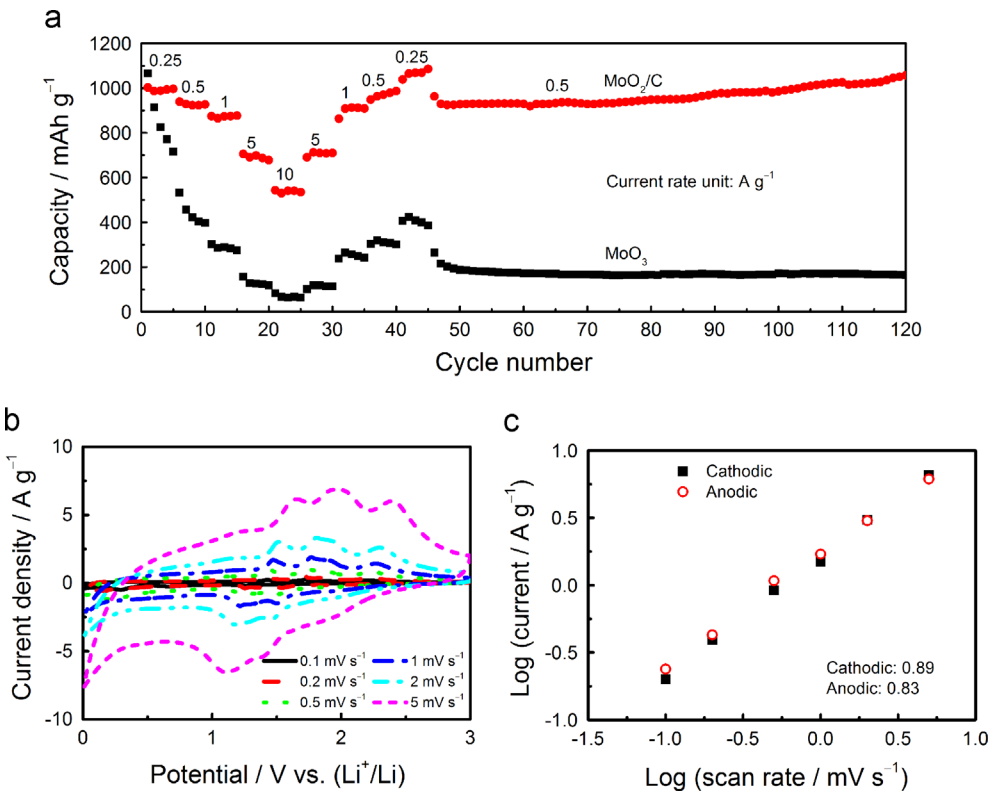

Figure 4 (a) Rate cycling performance of MoO_2/C and MoO_3 nanosheet electrodes. The electrode was first cycled at varied rates then at a constant rate of 0.5 A g^{-1}. (b) Cyclic voltammograms of MoO_2/C nanosheet electrode measured at various sweep rates. (c) Relationship between the peak currents due to Li insertion/extraction in MoO_2 nanosheets and scan rates in logarithmic format. Peak currents were collected from the redox pair due to orthorhombic phase transition to the monoclinic phase. The linear fitting ($R^2 > 0.996$) gives slopes of 0.89 and 0.83 for cathodic and anodic processes, respectively.

followed by thermal reduction by glucose. The structural features of a large surface area, enriched mesopores, ultrathin nanosheets and flexible carbon matrix endow the hierarchical material with superior Li storage capability. The resulting MoO_2/C nanosheets afford a high Li storage capacity of around 1030 mAh g^{-1}. In addition, they exhibit excellent high-rate capabilities, retaining 1051 mAh g^{-1} at 0.5 A g^{-1} over 100 cycles, and 719 mAh g^{-1} (86% of the available 838 mAh g^{-1}) at a much higher rate of 5 A g^{-1} for another 100 cycles. Rapid CV responses suggest that the Li storage in the MoO_2/C nanosheets involves intrinsically pseudocapacitive process. Such a superior capability suggests that ultrathin MoO_2 sheets hold tremendous potentiality for advanced rechargeable batteries.

Acknowledgments

Support of this work by the National Natural Science Foundation of China (51302181, 51372159, 51422206, and 51272197), the National Natural Basic Research Program of China (2013CB934103), and China Postdoctoral Science Foundation (2014M551647) is acknowledged. Liang Li would like to thank the support from 1000 Youth Talents Plan, and Distinguished Young Scholars (BK20140009) by Jiangsu Science and Technology Committee.

Appendix A. Supporting information

Supporting data associated with this article can be found in the online version at http://dx.doi.org/10.1016/j.nanoen.2014.10.027.

References

[1] J. Cabana, L. Monconduit, D. Larcher, M.R. Palacin, Adv. Mater. 22 (2010) E170-E192.
[2] D.O. Scanlon, G.W. Watson, D.J. Payne, G.R. Atkinson, R.G. Egdell, D.S.L. Law, J. Phys. Chem. C 114 (2010) 4636-4645.
[3] B. Hu, L. Mai, W. Chen, F. Yang, ACS Nano 3 (2009) 478-482.
[4] J.H. Ku, Y.S. Jung, K.T. Lee, C.H. Kim, S.M. Oh, J. Electrochem. Soc. 156 (2009) A688-A693.
[5] L. Zhou, H.B. Wu, Z. Wang, X.W. Lou, ACS Appl. Mater. Interfaces 3 (2011) 4853-4857.
[6] Y. Sun, X. Hu, W. Luo, Y. Huang, J. Mater. Chem. 22 (2012) 425-431.
[7] Q. Gao, L. Yang, X. Lu, J. Mao, Y. Zhang, Y. Wu, Y. Tang, J. Mater. Chem. 20 (2010) 2807-2812.
[8] L. Mai, F. Yang, Y. Zhao, X. Xu, L. Xu, B. Hu, Y. Luo, H. Liu, Mater. Today 14 (2011) 346-353.
[9] B. Guo, X. Fang, B. Li, Y. Shi, C. Ouyang, Y.-S. Hu, Z. Wang, G.D. Stucky, L. Chen, Chem. Mater. 24 (2012) 457-463.
[10] L. Yang, L. Liu, Y. Zhu, X. Wang, Y. Wu, J. Mater. Chem. 22 (2012) 13148-13152.

[11] Y. Shi, B. Guo, S.A. Corr, Q. Shi, Y.-S. Hu, K.R. Heier, L. Chen, R. Seshadri, G.D. Stucky, Nano Lett. 9 (2009) 4215–4220.
[12] X. Zhao, M. Cao, B. Liu, Y. Tian, C. Hu, J. Mater. Chem. 22 (2012) 13334–13340.
[13] Z. Wang, J.S. Chen, T. Zhu, S. Madhavi, X.W. Lou, Chem. Commun. 46 (2010) 6906–6908.
[14] L. Zeng, C. Zheng, C. Deng, X. Ding, M. Wei, ACS Appl. Mater. Interfaces 5 (2013) 2182–2187.
[15] X. Jiang, B. Tian, J. Xiang, F. Qian, G. Zheng, H. Wang, L. Mai, C.M. Lieber, Proc. Natl. Acad. Sci 108 (2011) 12212–12216.
[16] L.Q. Mai, B. Hu, W. Chen, Y.Y. Qi, C.S. Lao, R.S. Yang, Y. Dai, Z.L. Wang, Adv. Mater. 19 (2007) 3712–3716.
[17] W. Guo, C. Xu, G. Zhu, C. Pan, C. Lin, Z.L. Wang, Nano Energy 1 (2012) 176–182.
[18] Y. Sun, X. Hu, W. Luo, Y. Huang, ACS Nano 5 (2011) 7100–7107.
[19] K.H. Seng, G.D. Du, L. Li, Z.X. Chen, H.K. Liu, Z.P. Guo, J. Mater. Chem. 22 (2012) 16072–16077.
[20] J.H. Ku, J.H. Ryu, S.H. Kim, O.H. Han, S.M. Oh, Adv. Funct. Mater. 22 (2012) 3658–3664.
[21] J.W. Wang, Y. He, F. Fan, X.H. Liu, S. Xia, Y. Liu, C.T. Harris, H. Li, J.Y. Huang, S.X. Mao, Nano Lett. 13 (2013) 709–715.
[22] J. Liu, J. Jiang, C. Cheng, H. Li, J. Zhang, H. Gong, H.J. Fan, Adv. Mater. 23 (2011) 2076–2081.
[23] X.-L. Huang, R.-Z. Wang, D. Xu, Z.-L. Wang, H.-G. Wang, J.-J. Xu, Z. Wu, Q.-C. Liu, Y. Zhang, X.-B. Zhang, Adv. Funct. Mater. 23 (2013) 4345–4353.
[24] K.M. Hercule, Q. Wei, A.M. Khan, Y. Zhao, X. Tian, L. Mai, Nano Lett. 13 (2013) 5685–5691.
[25] W. Tian, X. Wang, C. Zhi, T. Zhai, D. Liu, C. Zhang, D. Golberg, Y. Bando, Nano Energy 2 (2013) 754–763.
[26] S. Hu, X. Wang, J. Am. Chem. Soc. 130 (2008) 8126–8127.
[27] S. Hu, X. Ling, T. Lan, X. Wang, Chem. Eur. J. 16 (2010) 1889–1896.
[28] Q. Huang, S. Hu, J. Zhuang, X. Wang, Chem. Eur. J. 18 (2012) 15283–15287.
[29] L. Kumari, Y.-R. Ma, C.-C. Tsai, Y.-W. Lin, S.Y. Wu, K.-W. Cheng, Y. Liou, Nanotechnology 18 (2007) 5717.
[30] J. Ni, G. Wang, J. Yang, D. Gao, J. Chen, L. Gao, Y. Li, J. Power Sources 247 (2014) 90–94.
[31] Y.S. Jung, S. Lee, D. Ahn, A.C. Dillon, S.-H. Lee, J. Power Sources 188 (2009) 286–291.
[32] W.-M. Chen, L. Qie, Y. Shen, Y.-M. Sun, L.-X. Yuan, X.-L. Hu, W.-X. Zhang, Y.-H. Huang, Nano Energy 2 (2013) 412–418.
[33] K. Chang, D. Geng, X. Li, J. Yang, Y. Tang, M. Cai, R. Li, X. Sun, Adv. Energy Mater. 3 (2013) 839–844.
[34] Y.-Y. Hu, Z. Liu, K.-W. Nam, O.J. Borkiewicz, J. Cheng, X. Hua, M.T. Dunstan, X. Yu, K.M. Wiaderek, L.-S. Du, Nat. Mater. 12 (2013) 1130–1136.
[35] Y.N. Ko, S.B. Park, K.Y. Jung, Y.C. Kang, Nano Lett. 13 (2013) 5462–5466.
[36] S. Ding, J.S. Chen, X.W. Lou, Chem. Eur. J. 17 (2011) 13142–13145.
[37] C. Xu, Y. Zeng, X. Rui, N. Xiao, J. Zhu, W. Zhang, J. Chen, W. Liu, H. Tan, H.H. Hng, Q. Yan, ACS Nano 6 (2012) 4713–4721.
[38] T. Brezesinski, J. Wang, S.H. Tolbert, B. Dunn, Nat. Mater. 9 (2010) 146–151.
[39] V. Augustyn, J. Come, M.A. Lowe, J.W. Kim, P.-L. Taberna, S.H. Tolbert, H.D. Abruña, P. Simon, B. Dunn, Nat. Mater. 12 (2013) 518–522.
[40] Y.G. Wang, Z.S. Hong, M.D. Wei, Y.Y. Xia, Adv. Funct. Mater. 22 (2012) 5185–5193.
[41] L. Zheng, Y. Xu, D. Jin, Y. Xie, J. Mater. Chem. 20 (2010) 7135–7143.
[42] J. Qiu, C. Lai, S. Li, S. Zhang, RSC Adv. 4 (2014) 18899–18903.
[43] J. Qiu, C. Lai, Y. Wang, S. Li, S. Zhang, Chem. Eng. J. 256 (2014) 247–254.

Jiangfeng Ni received his Ph.D. degree in Chemistry from Peking University in 2008. Then he worked at National Institute of Advanced Industrial Science and Technology in Japan and National University of Singapore until 2011. After that, he joined the College of Physics, Optoelectronics and Energy in Soochow University as an Associate Professor. Dr. Ni's research focuses on searching and developing high-performance functional materials for rechargeable lithium/sodium ion battery and supercapacitor applications.

Yang Zhao received his B.S. degree in Physics Science from Yancheng Teachers University in 2012. He is currently working toward the Master degrees at College of Physics, Optoelectronics and Energy in Soochow University. His scientific interests focuses on nanomaterials for non-aqueous lithium-ion batteries.

Liang Li received his Ph.D. degree from Institute of Solid State Physics, Chinese Academy of Sciences and won the Excellent President Scholarship in 2006. From 2007 to 2012, he worked in National University of Singapore, Singapore, National Institute of Advanced Industrial Science and Technology, Japan, National Institute for Materials Science, Japan, and the University of Western Ontario, Canada. Since August 2012, he is a full professor in Soochow University in China. His research group focuses mainly on the controlled synthesis, novel physical properties and nanoscale devices for energy-related applications. His publications have generated over 3000 citations. The H-index is 33.

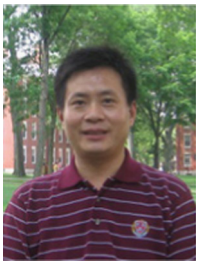

Liqiang Mai received his Ph.D. degree from Wuhan University of Technology in 2004. He then carried out postdoctoral research in the laboratory of Professor Zhonglin Wang at Georgia Institute of Technology in 2006–2007 and worked as an advanced research scholar in the laboratory of Professor Charles M. Lieber at Harvard University in 2008–2011. He is Chair Professor of Materials Science and Engineering at Wuhan University of Technology and Executive Director of the WUT-Harvard Joint Nano Key Laboratory. He has published more than 90 papers tagged by SCI in peer-reviewed journals such as Nature Nanotechnology, Nature Communications, Proceedings of the National Academy of Sciences, Journal of the American Chemical Society, Nano Letters, Advanced Materials. His interests include nanowire materials, micro/nanoenergy storage devices, and energy-based nano—bio interface.